



Thermo-mechanical investigation of the multi-layer thermocline tank for parabolic trough power plants

Karem Elsayed Elfeky ^{a,b,*}, Abubakar Gambo Mohammed ^a, Naveed Ahmed ^{c,d}, Qiuwang Wang ^{a,**}

^a Key Laboratory of Thermo-Fluid Science and Engineering, Ministry of Education, School of Energy and Power Engineering, Xi'an Jiaotong University, Xi'an, Shaanxi, 710049, PR China

^b Mechanical Engineering Department, Benha Faculty of Engineering, Benha University, Benha, 13511, Qalyubia, Egypt

^c US Pakistan Centre for Advanced Studies in Energy (USPCASE), National University of Sciences & Technology (NUST), H-12 Sector, Islamabad, Pakistan

^d Department of Energy and Petroleum Engineering, University of Stavanger, 4021, Stavanger, Norway

ARTICLE INFO

Keywords:

Cascaded layers tank
Plastic deformation
PCM melting temperature
Solar power plant
Thermal ratcheting

ABSTRACT

In applications of solar energy, thermal ratcheting is a crucial topic connected to the periodic performance of dual-phase thermocline storage tank. In order to investigate this phenomenon, a detailed simulation of a thermocline reservoir that includes both the hybrid tank wall and the varied filling zone is necessary. The thermo-mechanical characteristic of the cascaded layers storage tank for parabolic trough power plants is examined in the current work using one parametric study (dimensionless temperature difference) to determine the impact of changing the melting temperature of the phase change material (PCMs) layers. Experimental work from earlier studies is utilized to validate the numerical outcomes currently being presented. The results showed that structures-VIII and XIV have acceptable thermal performance, but ineffective mechanical performance since the normalized stress values were greater than one. The structure-XIII has the best overall efficiency of 79.58%, followed by structures-II, III, and XI, with performance levels of 70.82%, 67.83%, and 66.85%, respectively. The lowest overall efficiency attains by structure-XII, which equals 22.21%. The energy retrieved, overall efficiency, capacity ratio, and utilization ratio for the best scenario "structures- XIII" are 188.2 MWh, 79.58%, 44.34%, and 40.5%, respectively, based on the charging/discharging duration.

1. Introduction

Thermal energy storage (TES) has emerged as one of the most promising techniques with an increased focus on resolving energy shortages and lowering global greenhouse gas emissions [1]. Solar thermal energy [2], low grade waste heat [3], and industrial waste heat [4], are just a few examples of TES energy storage technology which utilizes heat storage materials as an energy storage medium. It can successfully address issues brought on by an asymmetrical distribution of time and space, as well as an imbalance among the demand and supply of energy [5]. With TES technology, a system's energy efficiency can be increased, peak electricity demand can be decreased, long-term financial and environmental benefits can be obtained, and energy utilization costs can be decreased [6].

Among the most potential large-scale renewable energy solutions are parabolic trough power (PTP) plants [7]. Energy storage options are necessary to deliver steady power generation, as PTP is susceptible to naturally occurring weather variations [8]. For PTP plants, a single dual-phase thermocline tank is a more affordable option than traditional multiple-tank systems [9]. As demonstrated in the literature, combining both fluid and solid into a single thermocline storage tank is emerging as a promising approach in this aspect [10]. The typical design is a dual-media container with heat transfer fluid (HTF) and an inert solid particle material, generally quartzite rock as well as silica sand [11], which serves as a porous medium. It is founded on the buoyancy stratification concept of dividing hot and cold fluid, with the first having a lower density at the top and the second having a higher density at the bottom. As a result, the HTF is introduced from the top tank part to perform a charging process (i.e., heating) and is discharged from the

* Corresponding author. Key Laboratory of Thermo-Fluid Science and Engineering, Ministry of Education, School of Energy and Power Engineering, Xi'an Jiaotong University, Xi'an, Shaanxi, 710049, PR China.

** Corresponding author.

E-mail addresses: karem_elfeky@xjtu.edu.cn (K.E. Elfeky), wangqw@mail.xjtu.edu.cn (Q. Wang).

Nomenclature		<i>Subscripts</i>	<i>Superscripts</i>	<i>Abbreviations</i>
A_{bed}	Bed cross-section area (m^2)	η	Energy efficiency	HTF Heat transfer fluid
c_p	Specific heat capacity ($\text{J}/(\text{kg}\cdot^\circ\text{C})$)	γ	Utilization ratio	PCMs Phase change materials
E_{store}	The tank's energy store (J)	ρ	Density (kg/m^3)	PCTs Phase change temperature
E_{pump}	Pumping energy (J)	σ	Capacity ratio	PTP Parabolic trough power
E_{input}	Charging energy (J)	k	Thermal conductivity ($\text{W}/(\text{m}\cdot^\circ\text{C})$)	TES Thermal energy storage
E_{retrieve}	Energy retrieved from the tank (J)			
g	Gravity (m/s^2)			
h_{fs}	The heat of fusion (J/kg)			
Nu	Nusselt number			
N_x	Nodes in the axial direction			
Pr	Prandtl number			
ΔP	Pressure drop (Pa)			
Ra	Rayleigh number			
Re	Reynolds number			
r	The radius of the PCM sphere (m)			
T_m	Melting temperature ($^\circ\text{C}$)			
ΔT	Temperature difference ($^\circ\text{C}$)			
t	Time (s)			
T_{ini}	Tank's initial temperature ($^\circ\text{C}$)			
u_f	Fluid velocity (m/s)			
x	Axial direction			
<i>Greek symbols</i>				
ε	Average bed porosity			
μ	Dynamic viscosity ($\text{kg}/(\text{m}\cdot\text{s})$)			
ν	Kinematic viscosity (m^2/s)			

lower tank section to complete a cooling process because the solid acts as the primary sensible heat storage media, the filler material's principal advantage is the decrease of higher-cost fluid needed [12]. These, along with using one tank rather than two, resulted in cost savings of about 33% as compared to the two-tank solar salt technique [13].

Despite its clear promise, there is still a serious issue that has prevented its use in industrial units [14]. It alludes to a phenomenon known as thermal ratcheting that could endanger the system's structural integrity [15]. It might happen if the designer repeatedly heats and cools the tank filled with solid particles. When heated, a radial gap between the wall and the filling substance is created as long as the wall has a higher thermal expansion than the filling substance. This allows the cohesionless particles to sink lower and fill the gap. Whenever the temperature reduces, the tank can not entirely contract, creating thermal stresses that could lead to plastic deformation. The tank wall will gradually ratchet outward until it breaks if strain hardening is unable to stop the same process in the subsequent heating and cooling cycles. Flueckiger et al. [14] used the static modeling approach to analytically study the stress characteristics under various limited circumstances for the investigations of the mechanical capabilities of the storage tank employing quartzite rock or silica sand as a solid filling. The findings demonstrated that by increasing insulation thickness, thermal ratcheting could be eliminated without experiencing a significant energy loss. A thorough parametric analysis of the combined thermo-mechanical effectiveness of the storage tank under constant circumstances was carried out by Wang et al. [16] using the aforementioned model. Additionally, González et al. [15] created a new mathematical model to assess the transient thermal-mechanical characteristics of a thermocline storage tank whenever the influences of the tank's inherent weight and high thermal gradient are disregarded. After analyzing how various criteria, including season weather variations, aspect ratio, and wall thickness, affected the stress properties, the tank's structure was optimized. Furthermore, Wan et al. [17] conducted a stress investigation on the TES tank with liquid sensible heat technology. They evaluated the

thermal and mechanical effectiveness of a hot tank, which is primarily used in concentrating solar power plant systems. They then made recommendations for the safety design of the tank, with a focus on the distribution of stress.

Moreover, this paragraph will explain some technology approaches that have been proposed to circumvent the thermal ratcheting problem. Flueckiger et al. [14] have suggested that the vessel should have a composite wall. In order to decrease the difference in wall temperature and, subsequently, the risk of ratcheting, it establishes an insulating layer among the interior and the metal shell. An underground concrete tank with a concave form has been constructed and modeled [18] to direct the rocks to ascend throughout the thermal expansion and thus lessen lateral pressure on the tank walls. Another idea involves removing all of the solid filling substance to create a single phase thermocline tank that contains only fluid [9]. Even while convective mixing fluxes are still considered in the absence of a porous medium, the thermal diffusivity decreases, allowing it to perform slightly better thermally. Another workable solution is an organized and packed thermocline tank [19]. In order to prevent the solid filler from settling, alternative configurations of structural material might be employed to substitute the packed aggregated bed [20]. All of these options have economics as their main drawback when compared to the original thermocline. Hoffmann et al. [21] conducted an experimental setup for the thermocline storage tank to assess the precision and computing efficiency of the single phase model against two phase approach. They examined the necessity of including heat losses as well as the tank wall in the calculation. They discovered that releasing the wall tank decreased computational efficiency by 13% but that it was necessary to include the wall in the simulation if the energy it contained exceeded 5% of the overall energy storage in order to produce accurate estimations of the heat transfer fluid over the tank elevation.

Even though thermocline tank heat transmission [8] sensible storage [22] and hybrid sensible-latent storage tank performance [23] have been extensively studied, few works have conducted a mechanical study

that solves the ratcheting problem. In order to prevent any plastic deformation, the testing equipment tank system of Solar One Pilot Plant [24] was designed using a tank wall made of a material with high yield strength. The inner gravel's active load and differential expansion with the shell were taken into consideration during development. The cooling from the greatest temperature to the surrounding temperature with a fictitious hard filler was investigated just for one specific stress state. No signs of thermal ratcheting were seen over the duration of these facilities' five-year operation, and tank wall hoop stress measurements were made [25]. Regrettably, they exhibited significant ambiguity, and no decision was made. The succeeding analyses have only utilized numerical modeling. The Solar One situation previously stated has been reproduced using a static stress-strain finite element calculation with different states of maximum and minimum operation conditions [26]. A stiff, cohesionless material without mass or thermal expansion was used to represent the solid in its simplest form. According to the elastoplastic numerical model, filler solid and shell have been more thoroughly examined in Ref. [27]. According to preliminary findings, physical bed characteristics are an important factor in overcoming ratchet failure. This has led to the establishment of experimental measures for specific bed properties. The dynamic growth of tank wall strains during a charging and discharging process was addressed in Ref. [28], but the thermal expansion of the particles was not taken into consideration.

In recent years, numerous computational methods have been used to thoroughly investigate the thermo-mechanical performance of the thermocline sensible heat storage tank in consideration of the studies mentioned above. However, no research has been done to look into the cascaded layer storage tank's thermo-mechanical effectiveness, considering the thermal expansion of the capsule. The current study's innovation investigates the impact of altering the melting temperature of phase change material's (PCMs) layers on the thermo-mechanical performance of the cascaded layers storage tank with a hybrid wall. In contrast to other research, this takes into account the thermal interaction between the main subsystem constituents, including the PCM capsule, insulation, fluid, environment, and shell. In this way, a thorough thermal loss calculation is carried out during the simulated plant and storage deal with actual operation and weather circumstances. The structural analysis is enhanced by utilizing a comprehensive model for the packing material that accounts for the thermal expansion of the capsules and tank solid mechanical behavior. In PTP plants that currently use a two tank energy storage subsystem called "Andasol [29]," the entire platform is used to simulate various thermocline tank arrangements. After the tank is properly designed for each scenario, a parametric study is initially performed to evaluate the efficiency of the storage and the risk of ratchet failure under typical operating conditions. According to the authors, there has not yet been a published presentation of the pairing of such a sophisticated, comprehensive model with this form of analysis. The current research enhances understanding of the cascaded storage tank's applicability to solar power facilities.

2. Mathematical and numerical model

In the following subsections for the two-phase mathematical model, the procedure by which the mathematical analysis is addressed using MATLAB will also be given in detail, as will the initial conditions and constraints. First, the structures and the material's characteristics will be described.

2.1. Issue description

Throughout this study, a two phase numerical approach has been constructed in which the storage tank is viewed as a porous, isotropic media composed of various sphere-shaped particles. The cascaded layers tank structure consists of a cylindrical tank that is positioned vertically and has two exits: one at the top and another at the bottom to be utilized for charging and discharging the solar salt. Inside the cascaded layers

tank, three unique PCMs layers are cascaded, each with a different phase change temperature (PCTs). A schematic illustration of the cascaded layers tank is presented in Fig. 1.

According to Fig. 1 and Table 1, structure-I is a cascaded storage tank including three distinct PCM layers that have different PCTs, such as high PCT^(KOH), intermediate PCT^(KNO₃), as well as low PCT^(NaOH), from the top down, respectively, wherein the tank's axial orientation is split into three equal portions. On the basis of changes in the dimensionless temperature difference (θ_m) of the three PCMs layers, the remaining fifteen structures have been hypothesized. All the thermophysical characteristics of the PCMs employed in the other fifteen constructions are constant; only the melting temperature varies using the θ_m , as illustrated in Table 2. The ongoing employment assesses the impact of a single parametric analysis for a hypothetical system of cascaded PCMs. The ideal melting temperature of the PCMs layers for a tank has been determined using this parametric analysis in order to boost the output energy from the storage tank and prevents the thermal ratcheting issue. This parameter allows the top, intermediate, or bottom portion of the cascaded layers tank to have different melting temperature values. Each PCMs layer's melting temperature is expressed in terms of its magnitude as follows: $T_p = \theta_m * (T_{h,f} T_{c,f}) + T_{c,f}$ [30].

where $T_{h,f}$ and $T_{c,f}$ represent, respectively, the charge and discharge temperatures of the HTF and T_p indicates the PCM capsule's temperature.

Table 3 summarizes the key characteristics of the current TES tank. Due to this, a convection heat transfer parameter from the PCMs capsules to the tank wall is required to connect the flow of solar salt with the high temperature in the tank casing. On the cylindrical tank wall, two potential solutions for the exterior boundary circumstances are taken into account. One of these solutions simulates a hybrid wall made of several layers, as seen in Fig. 1.

As indicated in Table 4, temperature-dependent functions are used to characterize density, viscosity, and thermal conductivity. Fig. 1 illustrates the several layers that make up the tank wall: an inside layer of firebrick for thermal isolation, a layer of steel for mechanical support, and an exterior layer of ceramic fiber for corrosion resistance and thermal isolation. Table 4 provides a summary of each layer's physical characteristics. As a result of the outer wall's exposure to the

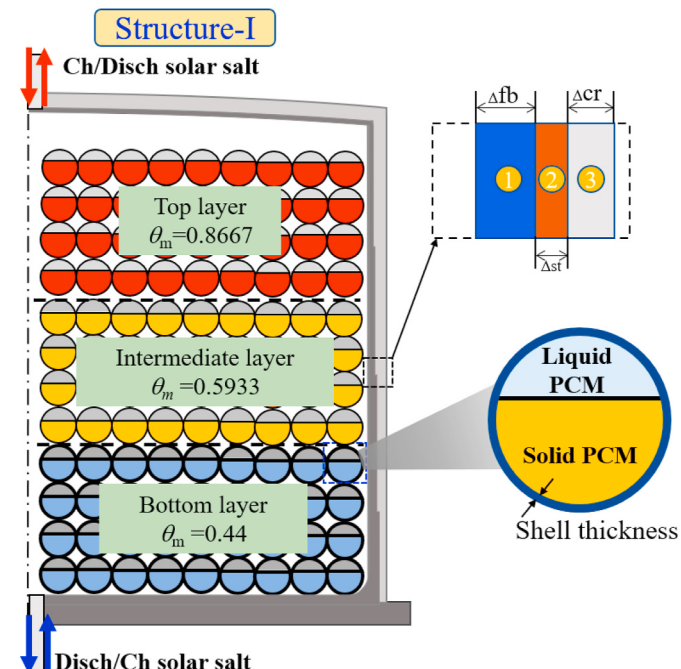


Fig. 1. A hybrid wall made of (firebrick (1), steel (2), and ceramic (3)) is shown schematically for the thermocline tank.

Table 1

Thermophysical characteristics of utilized PCMs.

Parameters	KOH [1, 31]	KNO ₃ [32]	NaOH [1]
Melting temperature (°C)	380	339	316
Latent heat (kJ/kg)	119	167	167
Specific heat capacity (kJ/kg. K)	Solid 1.47 Liquid 1.47	1.439 1.48	1385 1531
Density (kg/m ³)	Solid 2044 Liquid 2044	1900 1890	2097 2097
Heat conductivity (W/m.K)	Solid 0.5 Liquid 0.5	0.5 0.5	0.562 0.483

Table 2

The different configurations of the research subject.

Structures	θ_m			
	KOH	KNO ₃	NaOH	
I	0.8667	0.5933	0.44	
II	0.8	0.3	0.8	
III	0.8	0.8	0.2	
IV	0.6	0.55	0.2	
V	0.6	0.55	0.5	
VI	0.6	0.8	0.5	
VII	0.4	0.55	0.5	
VIII	0.4	0.3	0.2	
IX	0.4	0.8	0.8	
X	0.4	0.8	0.2	
XI	0.8	0.55	0.5	
XII	0.6	0.55	0.8	
XIII	0.8	0.8	0.8	
XIV	0.4	0.3	0.8	
XV	0.8	0.3	0.2	
XVI	0.6	0.3	0.5	

Table 3

Specifications and operating circumstances were employed [15].

Parameters	Value (unit)
Filler bed height (H)	10.5 (m)
Tank diameter (D_{bed})	19.55 (m)
Diameter of PCM capsule (d_p)	0.03 (m)
The porosity of the tank (ϵ)	0.4 (–)
PCM shell thickness	0.0005 (m)
Ceramic layer thickness Δc (m)	0.5 (m)
Steel layer thickness Δst (m)	0.06 (m)
Firebrick layer thickness Δfr	0.1 (m)
PCM shell thermal conductivity	13.94 (W/(m•°C))
HTF	Solar Salt
PCMs	KOH, KNO ₃ , NaOH
Working temperature ranges	290-390 (°C)

atmosphere, the thermal boundary conditions are based on a state of combined convection and radiation heat transfer.

The materials that are most frequently employed for TES at high temperatures are solar salt. The thermal stability of the materials used to store heat, or the range of temperatures where they are liquid, is the most crucial aspect influencing how well the TES system works. The heat can be stored across a wide range of extremely high temperatures thanks to the thermal stability of nitrate solar salt. 60% Sodium Nitrate (NaNO₃) and 40% Potassium Nitrate (KNO₃) make up the nitrate salt, often known as solar salt. Table 5 lists the solar salt's physical characteristics, which are well-known functions of temperature.

PCMs are chosen for the cascaded layer tank construction according to several factors that we have previously studied in depth [33]. The primary objective is to examine the impact of changing the melting temperature (dimensionless temperature difference) on the thermo-mechanical performance of the cascaded layers storage tank with a hybrid wall in order to choose the best structure which would

Table 4

The various wall layers and the capsule's physical characteristics.

Materials	Type	Symbol	Value
Capsule	Alumina, (Al ₂ O ₃)	ρ_{al} (kg/m ³)	3700
		$c_{p,al}$ (J/(kg.K))	1077
		k_{al} (W/(m.K))	16.734
		α (K ⁻¹)	8.10*10 ⁻⁶
		E (GPa)	300
		σ_y (MPa)	310
		$\nu(-)$	0.33
		ρ_{fr} (kg/m ³)	2000
		$c_{p,fr}$ (J/(kg.K))	1000
		k_{fr} (W/(m.K))	1
Wall	Firebrick	ρ_{st} (kg/m ³)	8000
		$c_{p,st}$ (J/(kg.K))	430
		k_{st} (W/(m.K))	60
		α (K ⁻¹)	1.35*10 ⁻⁵
		E (GPa)	200
		σ_y (MPa)	250
		$\nu(-)$	0.3
		ρ_c (kg/m ³)	1000
		$c_{p,c}$ (J/(kg.K))	1000
		k_c (W/(m.K))	1
Steel			
Ceramic			

Table 5

HTF's thermophysical characteristics [33].

Properties	Equation	Num.
Density (kg/m ³)	(- 0.6357 * T_{ave}) + 2089.9	(1)
Dynamic viscosity (kg.m.s)	((- 1.47 * 10 ⁻¹⁰) * (T_{ave}^3)) + ((2.28 * 10 ⁻⁷ - 10) * (T_{ave}^2)) - ((1.2 * 10 ⁻⁴ -) * T_{ave}) + 2.27 * 10 ⁻²	(2)
Specific heat (J/kg. K)	(0.172 * T_{ave}) + 1443	(3)
Thermal conductivity (W/m.K)	(0.00019 * T_{ave}) + 0.44299	(4)

maximize the energy stored or recovered from the tank and inhibit the thermal ratcheting concept for successive charging and discharging processes. The objective also includes evaluating the heat transfer characteristics of the sixteen cascaded layers tank. One parametric (dimensionless temperature difference) analysis is used to discuss how the thermo-mechanical performance of the cascaded layers tank fluctuates when the melting temperature of the PCMs layer changes [34].

2.2. Numerical equations

The thermal effectiveness of the cascaded layers tank structures in this investigation was evaluated by adopting the two phase numerical technique. By employing the two phase method, the tank with cascaded layers is considered to be an isotropic porous media composed of a variety of spherical shapes. A liquid envelope surrounds several particles that make up the storage tank. In this simulation analysis, it is assumed that the relationship for standalone PCMs capsules is identical to the relationship between the temperature distribution surrounding a PCM shell in the cascaded layers tank and the temperature inside the PCM capsule. The fluid phase's energy balance could be used to construct the differential equation for the distribution of shell temperatures. The sole method for addressing the thermal temperature dispersion across the PCM capsule is this approach. It is possible to formulate the energy conservation formulas Eq. (5) (solar salt), Eqs. (6) and (7). (both within and at the PCM capsule's perimeter). Additionally, the solar salt's passage through the packing zone is described using the current numerical model [35].

The first criterion presumes that the tank's interior and exterior sides are completely insulated; secondly, when charging and discharging, solar salt with a high intake temperature moves from the top to the lowest section of the cascaded layers tank, and the other way around.

Thirdly, the PCMs capsules are divided into precisely the exact distances and are given the same treatment. Fourth, the tank's emitted energy from both sides is overlooked by the existing two phase technique since it does not consider the influence of distributors due to its negligibility [36], and based on the inlet and exit temperatures, the solar salt's thermophysical properties can be calculated ($T_{\text{ave}} = (T_{\text{in}} + T_{\text{out}})/2$) [37]. Finally, internal heat generation has been disregarded.

The numerical approach used in this research, which is outlined in the following mathematical equations and the earlier-mentioned hypothesis, illustrates the process through which solar salt and PCMs capsules exchange heat:

Fluid phase [35]:

$$\varepsilon \rho_f c_{p,f} \frac{\partial T_f}{\partial t} + \varepsilon u_f \rho_f c_{p,f} \frac{\partial T_f}{\partial x} = \varepsilon k_f \frac{\partial^2 T_f}{\partial x^2} + h_f (T_s - T_f) + h_w (T_w - T_f) \quad (5)$$

where $c_{p,f}$ signifies solar salt's specific heat capacity, ρ_f denotes solar salt density, T_f indicates solar salt temperature, ε represents average bed porosity, u_f symbolizes solar salt inflow velocity, T_w denotes the temperature of the tank wall, h_w signifies the volumetric heat transfer parameter among cascaded layers tank and surroundings, k_f represents the solar salt's thermal conductivity, h_f indicates the volumetric heat transfer parameter among the solar salt and PCMs capsules, and T_s denotes the temperature of the PCM capsule.

Solid stage [35]:

$$(1 - \varepsilon) \rho_s c_{p,s} \frac{\partial T_s}{\partial t} = (1 - \varepsilon) k_s \frac{\partial^2 T_s}{\partial x^2} + h_f (T_f - T_s) \quad (6)$$

where the PCM's density, thermal conductivity, and specific heat are denoted by the symbols ρ_s , $c_{p,s}$, and k_s , respectively.

The outside surface of the PCM capsule's temperature change can be calculated using the formula below [35]:

$$\rho_s c_{p,s} \frac{\partial T_s}{\partial t} = \frac{1}{r^2} \frac{\partial}{\partial r} \left(k_s r^2 \frac{\partial T_s}{\partial r} \right) \quad (7)$$

where r represents the PCM capsule's radius.

The concept of efficient heat capacity is utilized to describe the phase shift's mechanism. Whenever the thermophysical characteristics of a cascaded layers tank change during the charging/and discharging operations. Within a particular temperature range ($\Delta T_m = T_{m2} - T_{m1}$), phase shift phenomena are expected to occur.

Beginning with the storage and recovery operations, the solid state could be calculated as follows [33]:

$$c_p = c_{p,s}, k_p = k_s, T_p < T_{m1} \quad (8)$$

where, λ_p denotes its thermal conductivity, and T_{m1} expresses the maximum temperature of the PCMs capsules throughout the solid-solid shift.

Additionally, the PCM capsule's stage transformation's progress during storage and recovery operations is calculated using Eq. (9) [33].

$$c_p = \frac{c_{p,s} + c_{p,L}}{2} + \frac{h_{fs}}{T_{m2} - T_{m1}} = \frac{c_{p,s} + c_{p,L}}{2} + \frac{h_{fs}}{\Delta T_m}, k_p = \frac{k_s + k_L}{2}, T_{m1} < T_p < T_{m2} \quad (9)$$

where, $c_{p,L}$ denotes liquid-specific heat capacity, k_L signifies the liquid stage's thermal conductivity, h_{fs} represents the heat of fusion, solid thermal conductivity is represented by the symbol k_s , T_{m2} denotes the maximum temperature of PCM throughout the solid to liquid shift, and solid specific heat capacity is indicated by $c_{p,s}$.

Furthermore, the following equation could be utilized to demonstrate the sensible liquid state during storage and recovery operations [33]:

$$c_p = c_{p,L}, k_p = k_L, T_p > T_{m2} \quad (10)$$

The coefficient of heat transfer among the fluid and the enclosed PCMs was calculated using a formula by Wakao et al. [38].

$$h_f = \frac{6(1 - \varepsilon)k_f}{d_p^2} \left(2 + 1.1 \left(Re^{0.6} Pr^{\frac{1}{3}} \right) \right); (15 < Re < 8500) \quad (11)$$

where, d_p denotes the PCM capsule's outside diameter, Pr signifies the Prandtl number, h_f represents the fluid heat transfer coefficient, Re indicates the Reynolds number and, k_f denotes the thermal conductivity of solar salt.

The comprehensive heat transfer coefficient indicates how much energy is lost through the hybrid tank wall to the environment (h_w). The calculation of this value takes into account the thermal resistance resulting from heat convection among the solar salt and inner tank wall, the conductivity through the composite tank wall, as well as convection and radiation outside the tank wall [39].

$$h_w = \frac{h'(\pi D_{\text{bed}})}{\pi D_{\text{bed}}^2 / 4} = \frac{4h'}{D_{\text{bed}}} \quad (12)$$

$$\frac{1}{h'} = \frac{1}{h_{in}} \frac{d_r}{D_{\text{bed}}} + \frac{D_{\text{bed}}}{2} \sum_{j=1}^n \frac{1}{k_{i,j}} \ln \frac{r_{j+1}}{r_j} + \frac{1}{h_{out}} \frac{r_r}{r_{n+1}} \quad (13)$$

where D_{bed} is the tank's diameter, j denotes the insulation layer indicator, k_j denotes the insulation layer's thermal conductivity, $j = 1$ denotes the interior tank wall, n denotes the sum of insulation sheets, h_{in} is the internal cascaded layers of the tank wall's parameter of heat loss.

Using a formula from Reference [37], the natural convection (h_{out}) on the exterior cascaded layers tank wall is computed.

$$h_{out} = \frac{Nu_{out} k_w}{H} = \frac{\left\{ 0.825 + 0.387 [Ra, f(Pr)]^{\frac{1}{16}} \right\}^2 k_w}{H} \quad (14)$$

where Nu represents the Nusselt number, k_w denotes the hybrid wall thermal conductivity, and H indicates the entire tank elevation.

$$f(Pr) = \left[1 + (0.492/Pr)^{\frac{9}{16}} \right]^{\frac{16}{9}} \quad (15)$$

$$Ra = Gr Pr \quad (16)$$

where Gr denotes the Grashof number, and Ra indicates the Rayleigh number.

$$Gr = g \beta \Delta T H^3 / \nu^2 \quad (17)$$

where ΔT denotes the temperature variance, β denotes the thermal expansion coefficient, g indicates gravity, and ν is a symbol for the kinematic viscosity.

On the interior surface of the cascaded tank, the coefficient of heat loss (h_{in}) was calculated using the Beek [40] equation.

$$h_{in} = \frac{\left[\left(0.203 Re_p^{1/3} Pr_p^{1/3} \right) + \left(0.220 Re_p^{0.8} Pr^{0.4} \right) \right] k_f}{d_p} \quad (18)$$

Effective conductivity can be explained in terms of the filling area arrangement and the thermal characteristics of the solid and liquid phases. The efficient thermal conductivity of the cascaded tank can be calculated using the Gonzo [41] formula.

$$k_{eff} = k_f \left[\frac{1 + 2\beta\varphi + (2\beta^3 - 0.1\beta)\varphi^2 + \varphi^3 0.05 \exp(4.5\beta)}{1 - \beta\varphi} \right] \quad (19)$$

where $\varphi = 1 - \varepsilon$ and $\beta = (k_s - 2k_f)/(k_s + 2k_f)$.

The heat diffusion equation, which includes the required parameters for each layer, predicts that heat will be carried by conduction from one layer of the hybrid wall to the next [15].

$$\frac{\partial(\rho_w c_{p,w} T_w)}{\partial t} = \nabla \cdot (k_w \nabla T_w) \quad (20)$$

where, $c_{p,w}$ represents its specific heat, k_w indicates its conductivity, and ρ_w denotes the wall's density. In order to account for temperature fluctuations throughout the circumference and height of the wall, both the axial (Δx) and radial (Δr) directions, the tank wall was segmented into intervals. $T_{w_{i,j}}$ is the temperature recorded in the center of the cell (i,j). The cell has a cylinder-shaped annular ring ($r_j - \Delta r/2 < r < r_j + \Delta r/2$ and $(x_i - \Delta x/2 < x < x_i + \Delta x/2)$.

Thermal conductance's used to describe how the cells are thermally coupled. The conductivity across cells ($i-1,j$) and (i,j) in the x-direction is as follows [42]:

$$K_{i-0.5,j} = \frac{2\pi r_j \Delta r}{\frac{0.5\Delta x}{k_{w_{i-1,j}}} + \frac{0.5\Delta x}{k_{w_{i,j}}}} \quad (21)$$

where $k_{w(i,j)}$ represents the cell's thermal conductivity (i,j), similarly, the conductivity across cells (i,j) and ($i+1,j$) is as follows:

$$K_{i+0.5,j} = \frac{2\pi r_j \Delta r}{\frac{0.5\Delta x}{k_{w_{i,j}}} + \frac{0.5\Delta x}{k_{w_{i+1,j}}}} \quad (22)$$

As the axial direction's heat conductivity is constant ($k_{w(i-1,j)} = k_{w(i,j)} = k_{w(i+1,j)}$), The following expression is the outcome of equation (22).

$$K_{i-0.5,j} = K_{i+0.5,j} = \frac{2\pi r_j \Delta r k_{w_{i,j}}}{\Delta x} \quad \text{for } i = 1, \dots, N \quad (23)$$

In the circular path across cells ($i,j-1$) and (i,j), the general equation for conductivity that applies to the interior nodes is as follows [42]:

$$K_{i,j-0.5} = \frac{\Delta x}{\frac{1}{2\pi k_{w_{i,j-1}}} \ln \frac{r_{j-0.5}}{r_{j-1}} + \frac{1}{2\pi k_{w_{i,j}}} \ln \frac{r_j}{r_{j-0.5}}} \quad \text{for } j = 2, \dots, M \quad (24)$$

as well as that among cells (i,j) and ($i,j+1$) being as follows:

$$K_{i,j+0.5} = \frac{\Delta x}{\frac{1}{2\pi k_{w_{i,j}}} \ln \frac{r_{j+0.5}}{r_j} + \frac{1}{2\pi k_{w_{i,j+1}}} \ln \frac{r_{j+1}}{r_{j+0.5}}} \quad \text{for } j = 1, \dots, M-1 \quad (25)$$

The solar salt is in the interface with the internal cell along the radial direction ($j = 1$); as a result, the thermal boundary condition of the interior cell is adjusted to a convection heat transfer state. As a result, the new Eq. (24) formula is as follows:

$$K_{i,0.5} = \frac{\Delta x}{\frac{1}{2\pi r_{in} h_{wi}} + \frac{1}{2\pi k_{w_{i,1}}} \ln \frac{r_{in}}{r_{in}}} \quad (26)$$

where h_{wi} represents the convective heat transfer from the capsule to the interior surface of the tank wall and r_{in} indicates the radius of the internal tank.

Due to the outer cell's exposure to the atmosphere towards the radial orientation ($j = M$), Its temperature boundary circumstance is configured to use a combined radiation and convection heat transfer criterion [42].

$$K_{i,M+0.5} = \frac{\Delta x}{\frac{1}{2\pi k_{w_{i,M}}} \ln \frac{r_{out}}{r_M} + \frac{1}{2\pi r_{out} h_{(out+rad)}}} \quad (27)$$

where $h_{out+rad}$ is the combined heat transfer by convection and radiation from the outside surface of the rank wall to the environment, and r_{out} is the outside tank radius.

Convective heat transfer from the exterior is covered in the section before, and radiative heat transfer was calculated as follows [42]:

$$h_{rad} = \epsilon_c \sigma_r (T_w^4(i.M) - T_\infty^4) \quad (28)$$

where ϵ_c presents the emissivity of the ceramic surface, σ_r indicates the Stefan-Boltzmann parameter, and T_∞ denotes the environmental

temperature.

The following formulas describe how much heat moves through a cell's top and bottom bounds ($Q_{i-0.5,j}$), and ($Q_{i+0.5,j}$), respectively.

$$Q_{i-0.5,j} = K_{i-0.5,j} (T_{w_{i-1,j}} - T_{w_{i,j}}) \quad (29)$$

$$Q_{i+0.5,j} = K_{i+0.5,j} (T_{w_{i,j}} - T_{w_{i+1,j}}) \quad (30)$$

In terms of heat flow, the boundaries with inner ($Q_{i-0.5,j}$) and outer ($Q_{i+0.5,j}$) radii are stated as follows:

$$Q_{i,j-0.5} = K_{i,j-0.5} (T_{w_{i,j-1}} - T_{w_{i,j}}) \quad (31)$$

$$Q_{i,j+0.5} = K_{i,j+0.5} (T_{w_{i,j}} - T_{w_{i,j+1}}) \quad (32)$$

For the purpose of obtaining the wall's temperature distributions, the energy conservation of the wall is addressed [15].

$$\rho_w c_{p,w} V \frac{\partial T_w}{\partial t} = Q_{i-0.5,j} - Q_{i+0.5,j} + Q_{i,j-0.5} - Q_{i,j+0.5} \quad (33)$$

where $V = 2\pi r_j \Delta r \Delta x$ indicates the cell volume.

As a result of the tank wall's three separate layers, the wall's characteristics (ρ_w , $c_{p,w}$, and $k_{w(i,j)}$) are unchanged along the radial direction. Consequently, for each layer, Eq. (33) must be calculated.

The change in pressure inside the cascaded layers tank structures is computed, per Ref. [43].

$$\Delta P = 150H \frac{(1-\varepsilon)^2}{\varepsilon^2} \frac{\mu_f u_f}{d_p^2} + 1.7H(1-\varepsilon) \frac{\rho_f u_f^2}{d_p} \quad (34)$$

where ΔP denotes the change in pressure between the tank's cascaded layers, and μ_f represents the fluid's dynamic viscosity.

2.3. Thermocline tank mechanical stress

The steel tank shell will swell or shrink as a result of temperature fluctuations that match those over the elevation of the tank's cascaded layers of the tank wall. As mentioned above, the internal volume of the tank grows during the charge half-cycle, and the spherical capsules settle down to occupy the extra space. Nevertheless, as the cascaded layers tank starts to cool during the recovery cycle because of the particles' internal friction and gravity, the spherical capsules cannot be relocated upward, which during repeated operating cycles gradually generates a rise in the circular mechanical stress in the casing of the hybrid steel tank. The wall will plastically distort if the stress exceeds the material's yield strength, which could then cause a buildup of ratchets and a potential cascaded layers tank structural collapse. The tank casing can, however, swell or shrink without restriction in the height orientation since there are no structural limitations in this direction. As a result, the tank experiences no axial mechanical stress. The enveloping strain, which is made up of both thermal strain (ϵ_T) and mechanical strain (ϵ_M), is the sole strain that may cause thermal ratcheting, according to this reference [14].

$$\epsilon_L(x) = \epsilon_T + \epsilon_M \quad (35)$$

The wall material's thermal expansion coefficient (α) determines how much strain is generated by heat [14].

$$\epsilon_T(x) = \alpha(T_w(x) - T_{w,ref}) \quad (36)$$

While the mechanical strain is defined by the steel's elastic modulus (E) and fundamental stresses (σ) [14].

$$\epsilon_M(x) = \frac{1}{E} (\sigma_{11} - \nu(\sigma_{22} - \sigma_{33})) \quad (37)$$

Although the weight of the filler bed does exert considerable pressure on the hybrid tank wall, it is insignificant in comparison to the hoop stress caused by the tank radius's ongoing expansion [14]. As a result,

only hoop stress needs to be included in Eq. (37)'s dependence on the mechanical strain. Throughout a storage half cycle, the hybrid tank wall achieves its highest temperature, resulting in the greatest thermal strain. As a result of the tank wall's ability to expand freely and the fact that the strain connected with the firebrick and ceramic parts is viewed as minor, the mechanical strain, on the other hand, is equal to zero. Due to their weakly connected block construction, these layers are unable to provide the filler region with any structural support. The tank wall is ratcheted to the shape it reaches the highest temperature, and the maximum amount of strain is maintained in the circumferential orientation since, as previously indicated, the tank wall cannot compress due to the rearranged filler. A portion of the thermal strain created during the charging period is transformed into mechanical stress after the tank has cooled. This mechanical stress peaks whenever the steel layer's temperature reaches its lowest temperature. The highest mechanical stress along a particular piece of the tank wall, which is defined by the greatest temperature fluctuations, can be explained as follows [14].

$$\sigma_{\max}(x) = E\varepsilon_{T,\max}(x) = E\alpha(T_{w,\max}(x) - T_{w,\min}(x)) \quad (38)$$

In order to maintain the required levels of safety and dependability, the peak mechanical stress cannot be greater than the yield strength (σ_y) of steel.

As was previously mentioned, filler pressure rises during discharge, which causes a rise in tank wall stress. All thermal strain reduction cannot shift to elastic strain and instead manifests as plastic deformation if wall stress increases over yield strength. Due to the inability to remove this tensile plastic strain, the subsequent heating strain will raise the total strain, causing the radius of the shell to grow. At that point, the procedure will restart after the rocks have settled down in the newly created gap. Each cooling cycle sets the yielding, and each heating cycle sets a radius increment. Final plastic deformation will eventually result in fissures and apparently a ratcheting failure. If the corresponding stress does not surpass yield strength, the strain reduced by temperature during the discharge period will be fully recompensed by elasticity and, conversely, during heating, with no plastic deformation occurring. The von Mises yield criteria, which may be applied to multidimensional issues involving ductile materials, predict yield by evaluating the comparable tensile stress against the yield strength of the material. The following is the definition of the equivalent safety factor versus yielding [15]:

$$FoS_{\text{static}} = \frac{\sigma_y}{\sigma_{eq}} \quad (39)$$

where yield strength is denoted by σ_y .

Following is a presentation of the results' steel standardized stress, in particular with respect to yield strength [15]:

$$\omega(x) = \frac{\sigma_{\max}(x)}{\sigma_y} \quad (40)$$

2.4. Constraints and the initial conditions

Solar salt at high temperatures fills the tank from the top as the thermocline is being charged, with a constant inflow velocity and temperature (T_h). Cool solar salt reaches the tank from the bottom throughout discharge with a consistent inlet velocity and temperature (T_c). In the following part, boundary constraints for solving the differential equation system formed by Eqs. (5)–(7) and (20) are covered.

2.4.1. Boundary conditions

The initial setting for the cascaded layers tank construction is a full discharge.

$$T_f = T_s \text{ at low section} \quad (41)$$

Fig. 2 provides a summary of the boundary conditions required for

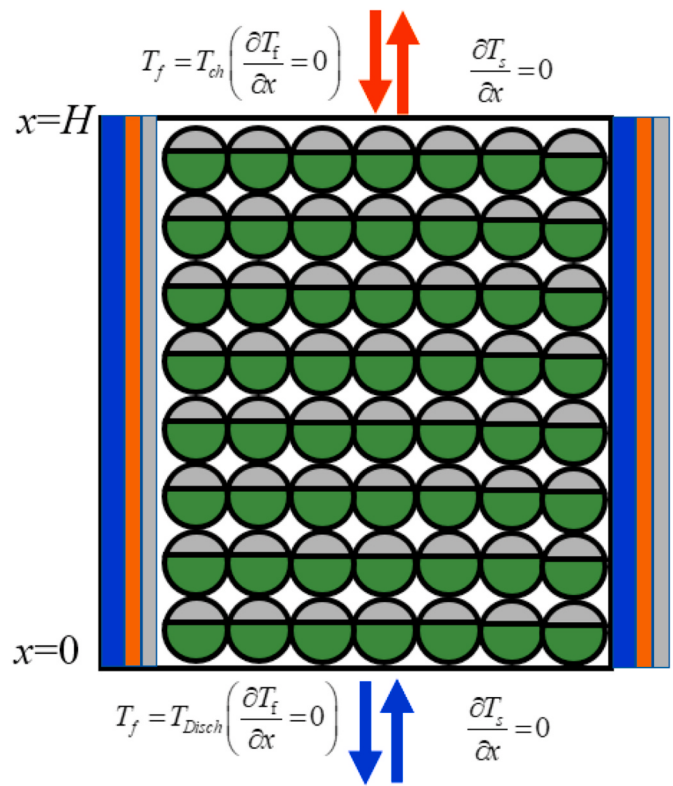


Fig. 2. Represents a description of the boundary circumstances for the hybrid wall, PCMs capsules, and the solar salt.

solving the arrangement of the differential formula defined by Eqs. (5)–(7) and (20).

The following calculations are made for the thermal limitations on the PCMs capsules' exterior and interior:

$$k_s \frac{\partial T_s}{\partial r} \Big|_{r=R_{s,i}} = h_p (T_f - T_s \Big|_{r=R_{s,i}}), \frac{\partial T_s}{\partial r} \Big|_{r=0} = 0 \quad (42)$$

The thermocline tank's ceramic outside encounters heat exchange with the surroundings by convection as well as radiation because of the hot solar salt inside:

$$\frac{\partial T_3}{\partial r} \Big|_w = -\frac{h_{out}}{k_3} (T_w - T_\infty) - \frac{\epsilon_w \sigma_r}{k_3} (T_w^4 - T_\infty^4) \quad (43)$$

2.4.2. Initial circumstances

For the first phase, it is crucial to identify the prerequisites. Since then, the fluid and PCMs capsules' starting temperatures for each subsequent recovery cycle have to be identical to how they were after each charging cycle. The operation factors are determined at the entrance and exit locations during the cascaded tank system's charging and discharging durations. Additionally, the temperature is checked frequently. To reduce the time needed for storage and recovery periods and to improve the fluidity of the analytical process, PCMs pills are regarded as isotropic. The tank's porosity does not change as the tank's elevation increases. This ensures that the rate at which fluid mass flows stays consistent during the movement of the filler zone. The two-phase numerical model is handled by the MATLAB code, which takes into account a one-dimensional numerical approach to the axial orientation of the tank.

2.5. Numerical approach

The filler region of the tank is divided into an identical number of control units. Additionally, for each case being considered right now, the

radial and axial orientations are split into a certain number of elements (R_x) and (N_x). The effectiveness of heat transfer between the encapsulated PCMs and the hot/cold fluid temperature affects how well heat is transferred between the two. By explicitly predicting the finite difference within the practical configuration, MATLAB is employed to solve the two phase modeling formulas that represent the heat transfer rate among encapsulated PCMs and the hot/cold fluid. The first-order upwind approach would be utilized in the mathematical formula (Eq. (5)) to satisfy the advective and temporal constraints concurrently. The diffusion concept would also be derived by applying the approach of second second-order difference. Additionally, concurrent resolution of the two phase mathematical technique is required. Through each phase, the solar salt's high and low temperatures are recorded for all thermo-mechanical performance indicators.

3. Performance analysis

The recovered energy, overall efficiency, utilization ratio, and capacity ratio of various configurations of the cascaded tank system have been summarized in Table 6. The results of earlier studies [30] provide more details regarding these equations.

4. Results and discussion

The model verification of the existing numerical model is provided first. Secondly, the temperature distributions for the storage and recovery cycles, the outflow temperature evolution, the thermal strain on the PCMs capsules and tank wall, and the hoop stress are all presented. Finally, the thermo-mechanical analysis of tank performance is covered.

4.1. Model validation

By evaluating the accurate numerical results generated by the present approach with the experimental data discovered through literature research, the accuracy of the proposed approach was examined. The present transient two phase computational model is first supported by the scientific research done by Wang et al. [47]. Wang et al. [47] experimental investigations for the thermocline tank were performed using air as the fluid and $\text{NaNO}_3\text{-KNO}_3$ (55–45 wt%) as the filler material. The primary numerical model's geometric parameters and working conditions for the cascaded layer tank employed in the suggested mathematical solution are identical to those presented in Wang et al. [47]. The outcomes of the numerical calculations are matched with the outcomes of the experiments, as depicted in Fig. 3, to confirm the

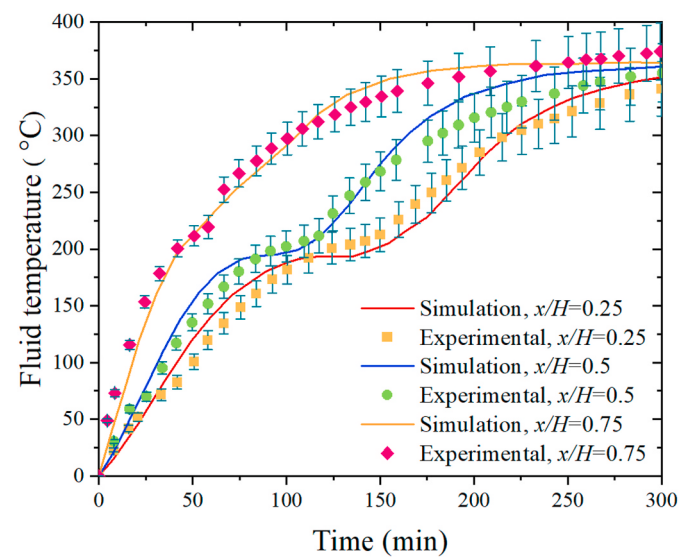


Fig. 3. Comparing the outcomes of the experimental measurements performed by Wang et al. [47] and the results produced by the current model proposed in this research.

correctness of the model. The temperature development of PCM capsules with storage time was computationally determined at sites in the packed bed where $x/H = 0.25, 0.5$, and 0.75 corresponded to the experimental temperature sampling locations. The temperature progression trend predicted by numerical simulations at various sites agrees well with the numerical measurement data, with a maximum deviation of 10.6%. The model can be considered valid in light of the numerical model's assumption and the intricacy of the experimental procedure.

The verifications provided strong support for further investigation into the thermal performance of the cascaded layers tank utilized in PTP facilities by demonstrating the validity of the proposed approach used for tank cycle computations. It is clear that the model is valid when the numerical model's assumption and the intricacy of the experimental procedure are taken into account. The inaccuracy is made worse by the ambiguity surrounding where thermocouples ought to be placed in the test rig. The general agreement between experimental and numerical data demonstrates the validity of the simulation analysis. This serves as the foundation for the numerical comparing results presented in the findings section.

Table 6

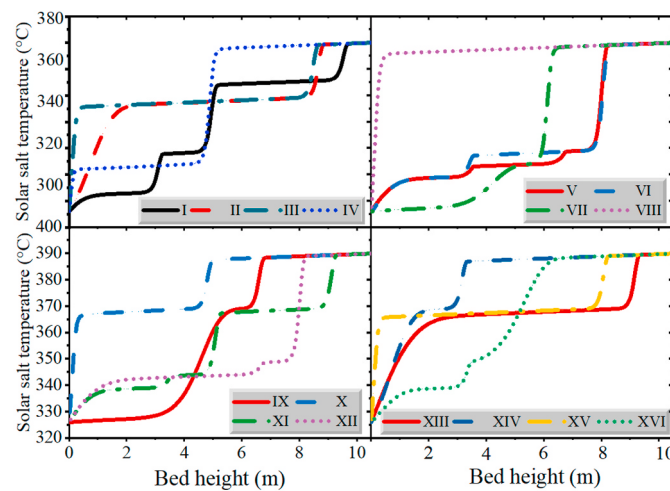
The equations are required to examine retrieved energy and the effectiveness of the simulation analysis [30,44–46].

Descriptions	Equations	Num.
Charging efficiency	$\eta_{ch} = \frac{E_{store}}{E_{ch} + E_{pump.ch}}$	(44)
Discharging efficiency	$\eta_{disch} = \frac{E_{retrieve}}{E_{store} + E_{pump.disch}}$	(45)
Overall efficiency	$\eta_{overall} = \eta_{ch} \times \eta_{disch}$	(46)
Stored or recovered energy	$E_{store/retrieve} = \begin{cases} \int_{T_{init}}^{T_p} (\rho c_p)_s dT & \text{if } T_p < T_{m1} \\ \int_{T_{init}}^{T_{m1}} (\rho c_p)_s dT + \int_{T_{m1}}^{T_p} (\rho c_p)_m dT + \rho_m \frac{(T_p - T_{m1})}{(T_{m2} - T_{m1})} h_{fs} & \text{if } T_{m1} \leq T_s \leq T_{m2} \\ \int_{T_{init}}^{T_{m1}} (\rho c_p)_s dT + \int_{T_{m1}}^{T_{m2}} (\rho c_p)_m dT + \rho_m h_{fs} + \int_{T_{m2}}^{T_p} (\rho c_p)_m dT & \text{if } T_p > T_{m2} \end{cases}$	(47)
Capacity ratio	$\sigma = \frac{E_{store}}{E_{store}^{\max}}$	(48)
Utilization ratio	$\gamma = \frac{E_{retrieve}}{E_{store}^{\max}}$	(49)
Maximum storage capacity	$E_{stored}^{\max} = m_{PCM} c_{p,L} (T_{in} - T_{m2}) + m_{PCM} h_{fs} + m_{PCM} c_{p,s} (T_{m1} - T_{ini})$	(50)

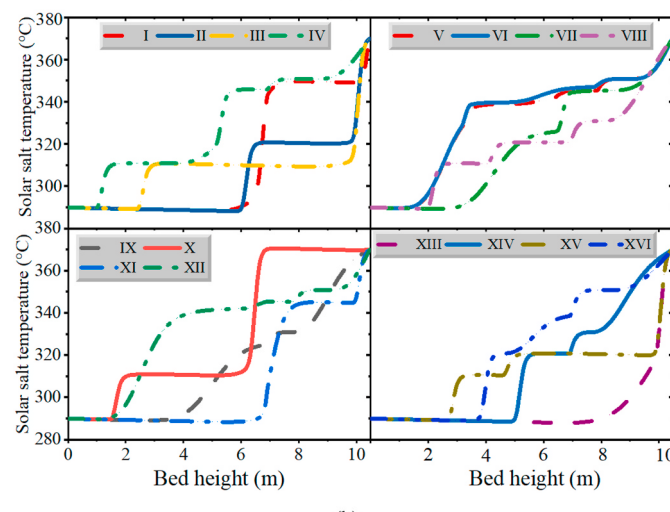
4.2. Temperature distributions for charging and discharging cycles

For all the investigated configurations, Fig. 4 depicts the axial temperature gradient of the hot and cold solar salt throughout the tank elevation during the storage and recovery phases. If a sequence of PCMs is utilized, each having a higher melting temperature than the subsequent, high heat transfer rates can be achieved. There are capsules holding PCMs with various melting temperatures at each phase. By doing so, this design creates a temperature difference between the PCMs and the hot/cold fluid that is more consistent. The rate of heat transmission between the hot/cold fluid and the PCMs capsules will increase during the charging and discharging operations anytime the PCMs layer is solidifying at a high temperature. The solar salt is released from the thermocline tank at the uppermost PCM layer's solidification temperature till it exceeds the discharge threshold temperature.

The melting temperature of each PCM layer has a significant impact on the temperature variation across the elevation of the cascaded layer tank during the charging phase, as shown in Fig. 4. The axial arrangement of the PCMs layers' melting and solidifying temperatures in the structure-VIII investigation closely matches the temperature of the hot fluid. Structure-VIII achieved the maximum thermal performance at the end of the charge cycle, as illustrated in Fig. 4(a), making it possible for it to store the most amount of energy conceivable in comparison to all other designs investigated. The structure-VIII thermal properties of the



(a)



(b)

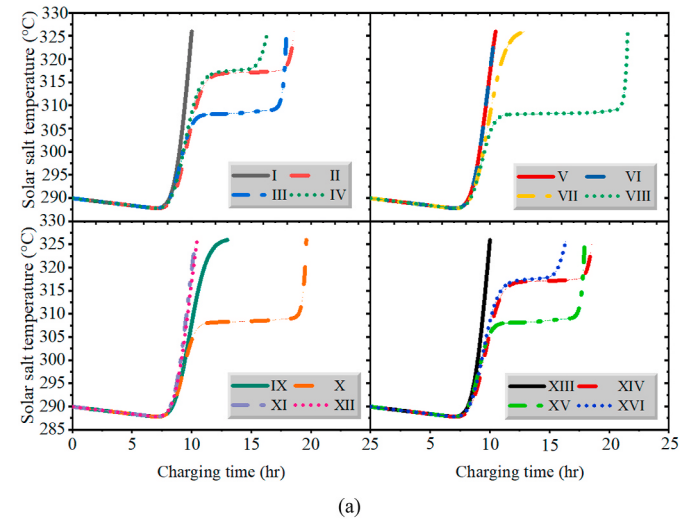
Fig. 4. The fluid's temperature gradient in axial flow around the tank's height during (a) charging and (b) discharge cycles.

design give coverage for 96.5% of the tank's elevation at high temperatures, but the structure-I "basic case" only offers 10.5% of the tank elevation at high temperatures throughout discharging period.

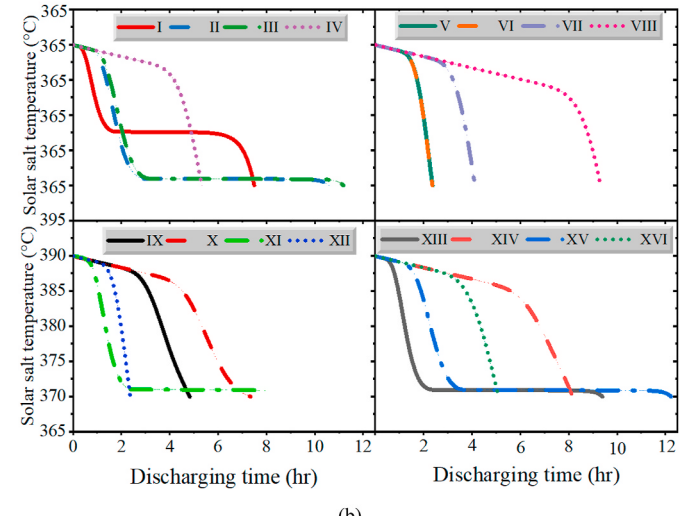
Structures V, VI, and XII are regarded to be among the worst structures since more than 75% of the elevation of the tank is within 345 °C during the storage cycle, which is classified as a lower temperature. While the configuration of the structure-XV is roughly the best scenario for the discharge mode because the phase transition process of the PCM occurs at 320 °C, which lengthens the recovery period as indicated in Fig. 5(b), the design of the structure-VIII is roughly the best case scenario for charging because it encompasses 96.5% of the tank elevation in a high temperature, as shown in Fig. 5(a).

4.3. Evolution of outflow temperature

Fig. 5 presents the distribution of fluid outflow temperature throughout the charging and discharging phases as a function of charge and release time for the chosen scenarios. The variance in temperature among the PCMs layers and the hot fluid during the charging process affects the heat transfer rate, and downstream portions of the bed are projected to have decreased heat transfer rates. A considerable heat transfer rate can be preserved by utilizing a series of PCMs along the bed



(a)



(b)

Fig. 5. Temperature profiles illustrate the outflow of solar salt over time throughout (a) storage and (b) recovery processes for various examined scenarios.

that has lowering melting temperatures. In order to achieve identical results during the unloading operation, the heat transfer fluid must travel in the reverse direction. The illustration illustrates the value of using TES tanks with cascaded layers of PCMs. The effectiveness of the cascaded layers tank configuration is affected by the " θ_m " of each PCM layer, as well as it influences how the tank's internal temperature is distributed throughout the storage and recovery processes. The tank can store a substantial amount of energy owing to the intermediate and bottom PCMs layers, which act as storage throughout the charging mode. The most significant level of thermal behavior for charging rounds is provided by structure-VIII, whereas the optimum level of thermal behavior for discharging cycles is provided by structure-XV. According to Fig. 5, structure-I displays the worst charging cycle, whereas structure-XII displays the worst discharging cycle. With arrangement-XV, the top PCM layer entirely melts before the interface breaks down, allowing the hot zone to penetrate all the way to the bottom of the cascaded layers tank. Furthermore, the PCM layer at the tank's base lowers the saturation level. This lengthens the tank's discharging period so that it can run longer and store more energy overall. In light of this, structure-XV has successfully stored the most energy.

The structure-XV has the greatest θ_m between the top, middle, and bottom PCMs layers throughout the discharging phase. Due to its capacity to discharge a significant amount of energy, as shown in Table 7, this instance displayed the best utilization ratio of all the investigated scenarios. Additionally, the results demonstrate that for the configurations under study, the charge and discharge time increases as the gap between the used PCM θ_m value grows. At the same threshold temperature, the structure-VIII has the longest charge time of 21.5 h, but the structure-XV has the greatest discharge time of 12.2 h. Furthermore, for the same boundary conditions temperature, the structure-XIII has a charge time of 10 h, which is the shortest, whereas the structure-XII has the shortest unloading time of 2.35 h. The optimum scenario for the charging and discharging phases depending on the retrieved energy is shown by structure-XV when all the analyzed configurations are taken into account and is entirely consistent with the previous findings.

4.4. PCMs capsules and tank wall thermal strain

Fig. 6 illustrates the evolution of the PCM capsule's thermal strain during the charging and discharging phases as a function of its circumference. The strain accumulation happens at the completion of the charge and discharge processes. According to the following

Table 7
The analyzed structure's tank overall performance characteristics.

Structures	Parameters				
	Charge/ Discharge time (hrs.)	Energy restored (MWh)	Overall efficiency (%)	Capacity ratio (%)	Utilization ratio (%)
I	10.3/7.48	159.48	65.96	47.37	37.22
II	13.55/	213.28	70.82	60.09	50.36
	10.56				
III	14.85/	225.7	67.83	69.86	57.12
	11.17				
IV	18.12/5.32	123.12	31.05	87.07	36.56
V	10.48/2.37	54.86	22.30	50.56	18.44
VI	10.45/2.35	54.52	22.21	50.18	18.13
VII	12.98/4.12	95.54	33.01	60.83	27.81
VIII	21.55/9.3	213.55	45.79	99.64	54.68
IX	12.98/4.8	109.64	37.88	60.30	30.13
X	19.6/7.33	165.05	38.60	92.32	46.06
XI	10.25/7.95	160.46	66.58	47.72	38.25
XII	10.47/2.35	54.53	22.19	50.26	18.07
XIII	10/9.38	188.20	79.58	44.34	40.50
XIV	18.6/8.16	186.43	47.59	80.64	46.03
XV	17.95/	247.83	62.87	84.91	65.25
	12.21				
XVI	16.37/5	117.19	33.43	73.95	32.48

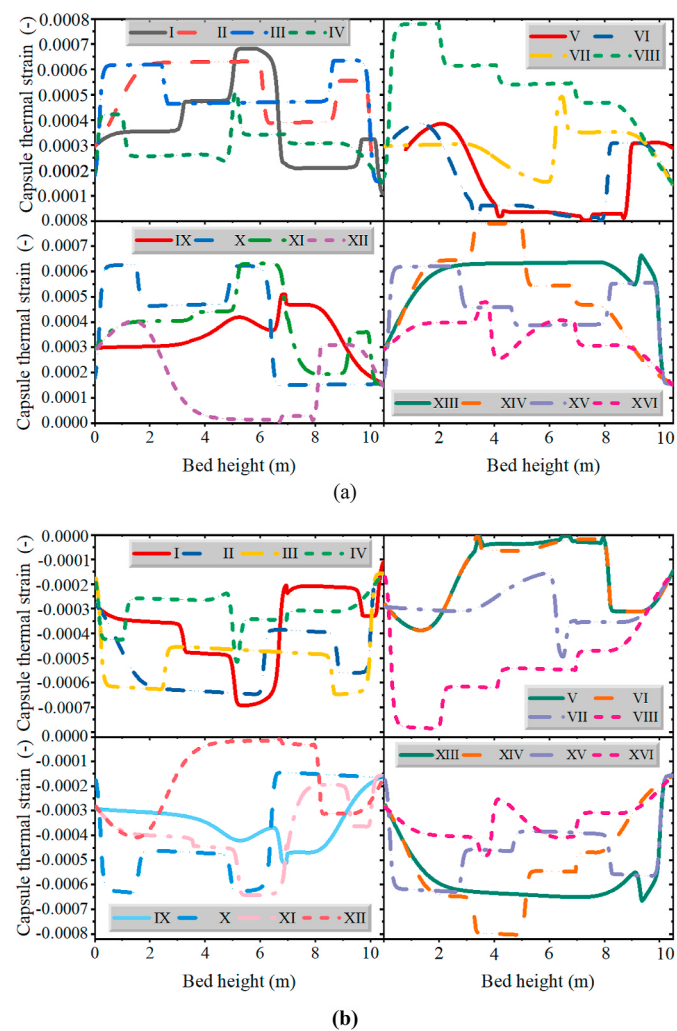
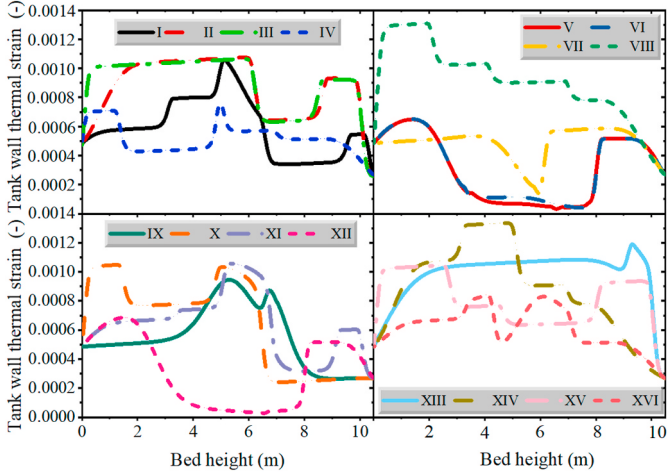


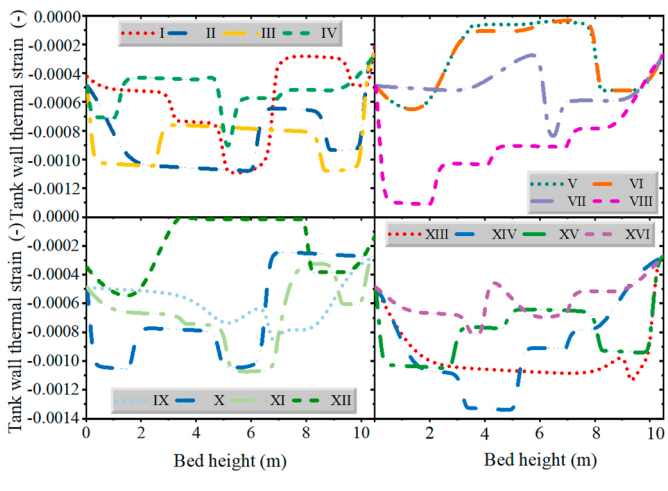
Fig. 6. The evolution of the PCM capsule's thermal strain during the (a) charging and (b) discharging phases.

explanation, the thermocline tank's PCM layer melting temperature is the primary factor determining the PCM capsule's maximum thermal strain. Their overall thermal strain may be at its maximum throughout charging and discharging periods if the cascaded thermocline tank arrangement is packed with PCM layers that have a high melting and solidification temperature. Due to the lengthy charging and discharging processes, the value of thermal strain gradually rises. The middle of the tank is typically where thermal strain tends to build up since the temperature of the PCM material there changes significantly at the completion of the storage and recovery processes. For this reason, structures-VIII and XIV exhibit the maximum thermal strain expansion along the tank throughout the storage and recovery stages, as illustrated in Fig. 6(a), and this expansion correlates to a contraction recovery period, as represented in Fig. 6(b).

In this section, Fig. 7 illustrates the evolution of the thermal strain of the tank wall during charging and discharging periods averaged over its perimeter. By the time the charging and discharging operations are complete, the strain begins to build up on the tank wall. The highest heat strain of the tank wall can be clarified in the following way, which depends depended on the heat losses to the surroundings: If the cascaded tank configuration has been stuffed with PCM layers with a high melting and solidification temperature, the total heat losses could be maximum during the storage and recovery durations due to the high rate of the heat transfer among the interior tank wall and HTF. Due to the lengthy storage and recovery periods, the value of the thermal strain of the wall



(a)



(b)

Fig. 7. Thermal strain on the tank height for the hybrid tank wall during (a) charging and (b) discharging cycles.

gradually rises. At the end of the storage and recovery periods, the temperature of the tank wall in this region considerably changes, it is common to see the accumulation of thermal strain mainly in the middle of the tank due to the thermal expansion coefficient of the tank wall ($\alpha_{\text{filler}} < \alpha_{\text{steel}}$), the overheating of the tank wall is larger than the entire PCM capsule in comparison to the thermal strain for the PCM capsule. Structures-VIII and XIV exhibit the maximum thermal strain expansion along the tank during the charging cycle, which is equal to 0.0013 and 0.00135, respectively, as shown in Fig. 7(a). This expansion correlates to a contraction throughout the discharge cycle, as depicted in Fig. 7(b).

4.5. PCM capsule and tank wall hoop stress

Fig. 8 shows the normalized stress values for the PCMs capsules during the discharging cycle for all sixteen scenarios. The difference in PCMs capsules melting temperature throughout the tank height is correlated with the maximum hoop stress of the PCMs capsules. Structure-XII had the shortest discharge time and the shortest normalized stress value among these structures. Structure-VIII, in contrast, has the longest discharging time and provides the highest normalized peak stress value. The surface of the PCMs capsules' temperature gradient responds to θ_m , which causes this behavior.

Additionally, it should be observed that all scenarios result in normalized maximum stress values that are smaller than one, with

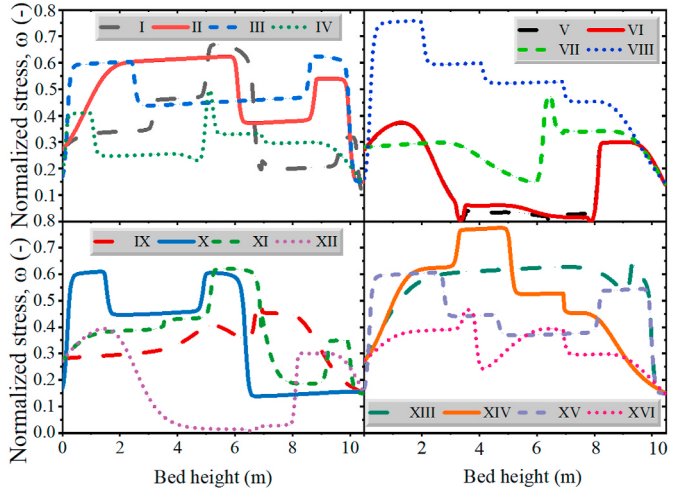


Fig. 8. Tank height hoop stress for the PCMs capsules.

structures I through XVI grouped between 0.407 and 0.76. Therefore, none of these scenarios would include the PCMs capsules ratcheting due to plastic deformation. Structure-XV might offer the best scenario because it recovers the most energy, which means thermal ratcheting is not a concern.

Fig. 9 shows the normalized stress data for the tank wall throughout the discharging cycle for all sixteen structures. The amount of heat lost at the cascaded layers of the tank surface throughout the tank height directly relates to the maximum hoop stress of the hybrid tank wall. Among these scenarios, structure-XV generates the highest normalized peak stress value and suffers the most heat losses from the tank wall during discharge. Additionally, the structure-XII creates the lowest normalized peak stress value and experiences the least heat losses from the tank. This phenomenon results from the PCMs capsule surface's temperature distribution being reactive to θ_m . It is also noticed that, with the exception of both structures-VIII and XIV, all scenarios result in normalized maximum stress values lower one, with structures I-VII, IX-XIII, and XV-XVI aggregated between 0.42 and 0.815. Even if the hybrid tank wall does not experience extremely high stress levels in structure-IX, more stress reductions may be able to optimize the thermal ratcheting factor of safety in the case of unanticipated raises in heat loss or other unforeseeable events. Consequently, structures VIII and XIV would experience ratcheting associated with plastic deformation for the tank wall as they give normalized peak stress values that are more than one. Additionally, compared to structure-VIII, structure-XV's peak stress is

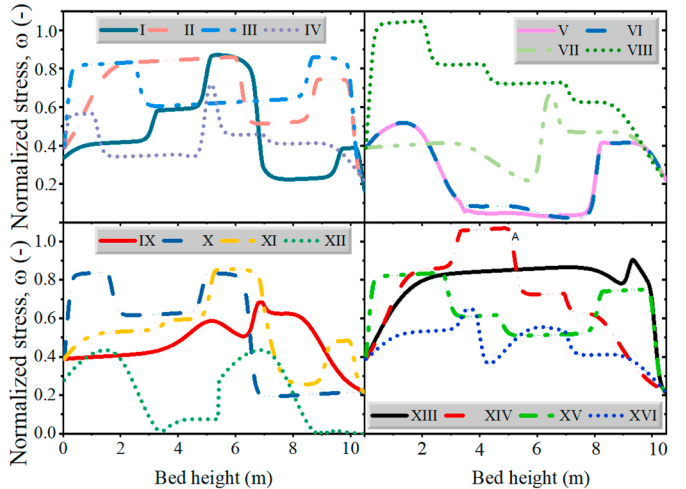


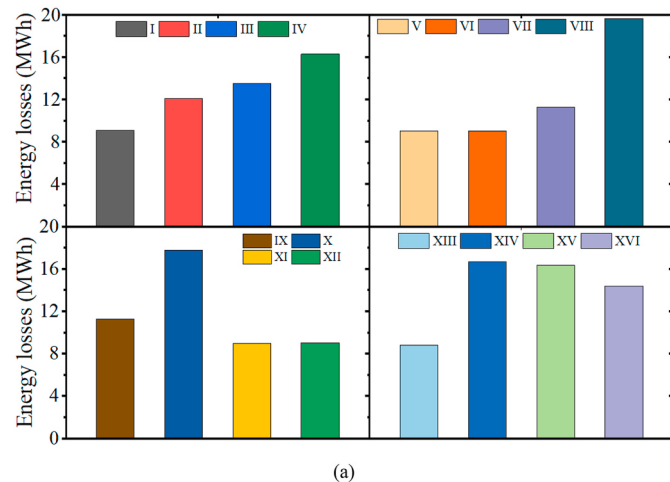
Fig. 9. Tank wall hoop stress on the tank's elevation.

18.6% lower. Due to the highest amount of recovered energy, structure-XV might present the ideal scenario given the problem of thermal ratcheting.

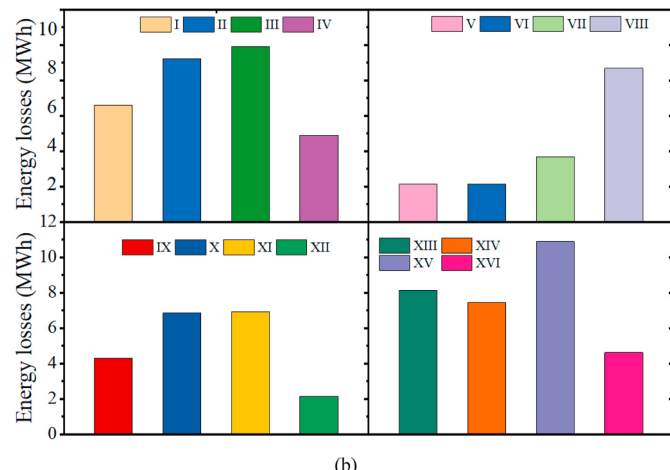
4.6. Assessment of tank performance

In Fig. 10, it is depicted how much energy is lost from the cascaded layers tank throughout the storage and recovery cycles for various thermocline tank structures. The quantity of energy lost from the cascaded tank's surface increases as storage and recovery times lengthen. As a result, at the end of the charging cycle, the quantity of energy lost from the tank surface for structure-VIII was roughly twice that of the structures-I, V, VI, XI, XII, and XIII, as shown in Fig. 5(a). According to Fig. 5(b), the quantity of energy lost from the cascaded tank's surface throughout discharge when there is a big θ_m difference between the top and middle PCM layer as in the structure-XV is more than that of other structures under the same boundary condition. According to Fig. 5, structure-VIII experiences the highest heat losses during the charging period at 19.66 MWh, whereas structure-XIV experiences the highest losses during the discharging process at 10.89 MWh.

For each configuration under investigation, Table 7 displays the recovered energy, charge and discharge duration, capacity ratio concerning overall efficiency, and utilization ratio. The study also shows that the restored energy for the configurations under study increases with the rise in the PCM layer's θ_m difference, with structure-XV



(a)



(b)

Fig. 10. The tank wall's energy lost throughout the (a) storage and (b) recovery cycles.

scenarios showing the most recovery when the θ_m value ranges from (0.8, 0.3, 0.2), which is equal to 247.83 MWh. Under the same boundary circumstances, structure-III has the second-highest recovered energy of 225.7 MWh, while structures-V, VI, and XII have the lowest recovered energy of 54.86, 54.52, and 54.53 MWh, respectively. As a consequence, the findings show that raising the top PCM layer's θ_m value improves overall efficiency throughout the charging and discharging phases. The structure-XIII has the best total efficiency of 79.58%, followed by structures-II, III, and XI, with performance levels of 70.82%, 67.83%, and 66.85%, respectively. The lowest overall efficiency attains by structure-XII, which equals 22.21%.

Moreover, Table 7 displays additional performance metrics for the TES configurations under study. The fluctuation of the TES thermocline tank's capacity ratio and utilization ratio during the charging and discharging phases have been thoroughly covered in Table 7. The amount of energy that can be stored in the cascaded layers tank varies and is based on the θ_m of each PCM layer. With a capacity ratio of 99.64%, structure-VII has the highest value. Structure-XIII shows a capacity ratio of 44.34%, which is the lowest result recorded.

In contrast, the structure-XV, which exhibits a utilization ratio of 65.25%, shows the most significant increase in terms of the utilization ratio. The structure-XII configuration indicates the lowest utilization ratio of 18.07%. The performance of the cascaded layers tank height as a whole throughout the charging and discharging operation is significantly impacted by the θ_m of the PCM layer. The optimal scenario for the charging and discharging phases depending on the retrieved energy can be seen in structure-XV when all the analyzed structures are taken into account, which is entirely consistent with the previous findings.

5. Conclusions

Investigating the thermo-mechanical performance of the cascaded layer thermocline tank throughout storage and release cycles is the main objective of the current work. The thermo-mechanical performance of the tank with a hybrid wall will also be examined, as will the impact of varying the melting temperatures of each PCM layer. In pursuance of avoiding reduction in heat transfer, temperature declines throughout the recovery period, and the thermal ratcheting phenomenon for successive storage and recovery operations, the present investigation compares and investigates the influence of varying the PCM layer melting temperature for the cascaded layers tank structure. It also evaluates the heat transfer performance of the sixteen combinations. For a comparative thermo-mechanical analysis, simulation results depend on a two phase numerical technique utilized. The mathematical model formulas were calculated using MATLAB code, and the present numerical findings have been confirmed. The suggested layout of the sixteen cases is contrasted with the base structure from the perspective of thermo-mechanical analysis considerations.

The main significant findings of the present investigation are discussed in the sections that follow.

- (1) The thermo-mechanical performance of the elevation of the cascaded layers tank throughout storage and release is significantly influenced by the PCM layer's θ_m .
- (2) The structure-VIII has the longest charging time of 21.5 h, while structure-XII has the shortest charging time of 10 h. Furthermore, the longest discharging time of 12.2 h was for the structure-XV, while the shortest charging time of 2.35 h was for the structure-XII.
- (3) Structures-VIII and XIV exhibit the maximum thermal strain along the tank during the charging cycle, equal to 0.0013 and 0.00135.
- (4) In addition, structures I-VII, IX-XIII, and XV-XVI have normalized maximum stress aggregated between 0.42 and 0.815, but structures VIII and XIV would experience ratcheting associated with plastic deformation for the tank wall as ($\omega > 1$).

- (5) While structure XIV has the largest heat losses during the recovery cycle with 10.89 MWh, structure-VIII experiences the most heat losses during the storage cycle with 19.66 MWh.
- (6) The structure-XIII has the best overall efficiency of 79.58%, followed by structures-II, III, and XI, with performance levels of 70.82%, 67.83%, and 66.85%, respectively. The lowest overall efficiency attains by structure-XII, which equals 22.21%.
- (7) In comparison to all other structures investigated in sequence, the capacity ratio of structure-VII is greater by 252.46, 39.69, 29.89, 12.62, 49.26, 49.64, 38.95, 39.48, 7.35, 52.11, 49.56, 55.50, 19.07, 14.78, and 25.78%.
- (8) Based on the charging/discharging period, the energy recovered, overall efficiency, capacity ratio, and utilization ratio for the best scenario “structures- XIII” are 188.2 MWh, 79.58%, 44.34%, and 40.5%, respectively.

Our present study focuses on the impact of altering the melting temperature of the PCM layers on the thermo-mechanical performance of the cascaded layers storage tank with a hybrid wall, one of the three major parts of the PTP plant, together with the solar collector and power block. The PCMs layers’ effective operating temperature ranges are the most important factors in the design of the storage tanks used in PTP systems. By supporting the ongoing research, another challenge is the assessment, research, and design of charging and discharging regulate strategies to optimize the thermo-mechanical performance of the tank while taking into account the entire design parameters of the PTP plant (solar collector, thermal storage system, and power plant) under various meteorological conditions.

Credit author statement

Karem Elsayed Elfeky: Conceptualization, Methodology, Investigation, Formal analysis, Validation, Writing - original draft, and Project administration. Abubakar Gambo Mohammed: Investigation, Validation. Naveed Ahmed, Investigation, Validation, Writing-Reviewing. Qiuwang Wang: Supervision, Writing-Reviewing, Editing, and Project administration.

Declaration of competing interest

The authors declare that they have no known competing financial interests or personal relationships that could have appeared to influence the work reported in this paper.

Data availability

No data was used for the research described in the article.

Acknowledgments

This work is financially supported by the Fundamental Scientific Research Expenses of Xi'an Jiaotong University (xzy012021021), the National Natural Science Foundation of China (Grant No. 51536007), and the National Natural Science Foundation of China (NSFC)/Research Grants Council (RGC) Joint Research Scheme (Grant No. 51861165105).

References

- [1] Banerjee B, Chatterjee S, Datta J, Saha SD. Application of phase changing materials in a CSP plant for thermal energy storage: a review on recent developments. Mater Today Proc 2022;62:3502–7.
- [2] Elfeky KE, Mohammed AG, Wang Q. Thermo-economic evaluation of PCM layer thickness change on the performance of the hybrid heat storage tank for concentrating solar power plants. Energy 2022;253:124128.
- [3] Guo F, Zhu X, Li P, Yang X. Low-grade industrial waste heat utilization in urban district heating: simulation-based performance assessment of a seasonal thermal energy storage system. Energy 2022;239:122345.
- [4] Manente G, Ding Y, Sciacovelli A. A structured procedure for the selection of thermal energy storage options for utilization and conversion of industrial waste heat. J Energy Storage 2022;51:104411.
- [5] Thanganadar D, Fornarelli F, Camporeale S, Asfand F, Gillard J, Patchigolla K. Thermo-economic analysis, optimisation and systematic integration of supercritical carbon dioxide cycle with sensible heat thermal energy storage for CSP application. Energy 2022;238:121755.
- [6] Liu T, Yang J, Yang Z, Duan Y. Techno-economic feasibility of solar power plants considering PV/CSP with electrical/thermal energy storage system. Energy Convers Manag 2022;255:115308.
- [7] Moreno-Tejera S, Silva-Pérez MA, Ramírez-Santigosa L, Lillo-Bravo I. Evaluation of classification methods according to solar radiation features from the viewpoint of the production of parabolic trough CSP plants. Renew Energy 2018;121:429–40.
- [8] Elfeky KE, Mohammed AG, Wang Q. Influence of inlet temperature on the performance of cascade and hybrid storage tank for CSP plants. Appl Therm Eng 2022;206:118098.
- [9] Mira-Hernández C, Flueckiger SM, Garmella SV. Comparative analysis of single- and dual-media thermocline tanks for thermal energy storage in concentrating solar power plants. J Sol Energy Eng 2015;137(3).
- [10] Cocco D, Serra F. Performance comparison of two-tank direct and thermocline thermal energy storage systems for 1 MWe class concentrating solar power plants. Energy 2015;81:526–36.
- [11] Elfeky KE, Mohammed AG, Wang Q. Performance analysis of an air rock thermocline TES tank for concentrated solar power plants using the coupled DEM-CFD approach. Clean Technol Environ Policy 2022;24(1):3–19.
- [12] Lou W, Xie B, Aubril J, Fan Y, Luo L, Arrivé A. Optimized flow distributor for stabilized thermal stratification in a single-medium thermocline storage tank: a numerical and experimental study. Energy 2023;263:125709.
- [13] Elfeky KE, Mohammed AG, Ahmed N, Lu L, Wang Q. Thermal and economic evaluation of phase change material volume fraction for thermocline tank used in concentrating solar power plants. Appl Energy 2020;267:115054.
- [14] Flueckiger S, Yang Z, Garmella SV. An integrated thermal and mechanical investigation of molten-salt thermocline energy storage. Appl Energy 2011;88(6):2098–105.
- [15] González I, Pérez-Segarra CD, Lehmkuhl O, Torras S, Oliva A. Thermo-mechanical parametric analysis of packed-bed thermocline energy storage tanks. Appl Energy 2016;179:1106–22.
- [16] Wang G, Yu S, Niu S, Chen Z, Hu P. A comprehensive parametric study on integrated thermal and mechanical performances of molten-salt-based thermocline tank. Appl Therm Eng 2020;170:115010.
- [17] Wan Z, Wei J, Qaisrani MA, Fang J, Tu N. Evaluation on thermal and mechanical performance of the hot tank in the two-tank molten salt heat storage system. Appl Therm Eng 2020;167:114775.
- [18] Zanganeh G, Pedretti A, Zavattini S, Barbato M, Steinfeld A. Packed-bed thermal storage for concentrated solar power—Pilot-scale demonstration and industrial-scale design. Sol Energy 2012;86(10):3084–98.
- [19] Duan Z, Zhang Z, Wang J, Cao X, Zhang J. Thermal performance of structured packed bed with encapsulated phase change materials. Int J Heat Mass Tran 2020; 158:120066.
- [20] Motte F, Bugler-Lamb S, Falcoz Q, Py X. Numerical study of a structured thermocline storage tank using vitrified waste as filler material. Energy Proc 2014; 49:935–44.
- [21] Hoffmann J-F, Fasquelle T, Goetz V, Py X. A thermocline thermal energy storage system with filler materials for concentrated solar power plants: experimental data and numerical model sensitivity to different experimental tank scales. Appl Therm Eng 2016;100:753–61.
- [22] Parida DR, Advaith S, Dani N, Basu S. Assessing the impact of a novel hemispherical diffuser on a single-tank sensible thermal energy storage system. Renew Energy 2022;183:202–18.
- [23] Ahmed N, Elfeky K, Qaisrani MA, Wang Q. Numerical characterization of thermocline behaviour of combined sensible-latent heat storage tank using brick manganese rod structure impregnated with PCM capsules. Sol Energy 2019;180: 243–56.
- [24] Gervais R. Central receiver solar thermal power system. Phase 1. CDRL item 2; Pilot Plant preliminary design report. Volume II. System decription and system analysis. Huntington Beach, Calif.(USA): McDonnell Douglas Astronautics Co.; 1977.
- [25] Faas S. 10-mwe solar-thermal central-receiver pilot plant: thermal-storage-subsystem evaluation-subsystem activation and controls testing phase. Livermore, CA (United States): Sandia National Lab.(SNL-CA); 1983.
- [26] Flueckiger SM, Yang Z, Garmella SV. Thermomechanical simulation of the Solar One thermocline storage tank. J Sol Energy Eng 2012;134(4):041014.
- [27] Kolb GJ, Lee G, Mijatovic P, Valmianski E. Thermal ratcheting analysis of advanced thermocline energy storage tanks. Albuquerque, NM (United States): Sandia National Lab.(SNL-NM); 2011.
- [28] González I, Lehmkuhl O, Pérez-Segarra C, Oliva A. Dynamic thermoelastic analysis of thermocline-like storage tanks. Energy Proc 2015;69:850–9.
- [29] Hermann U, Geyer M, Kistner R. The andasol project—workshop on thermal storage for trough power systems. Solar Millennium AG; 2002.
- [30] Elfeky K, Li X, Ahmed N, Lu L, Wang Q. Optimization of thermal performance in thermocline tank thermal energy storage system with the multilayered PCM (s) for CSP tower plants. Appl Energy 2019;243:175–90.
- [31] Galione PA, Pérez-Segarra CD, Rodríguez I, Oliva A, Rigola J. Multi-layered solid-PCM thermocline thermal storage concept for CSP plants. Numerical analysis and perspectives. Appl Energy 2015;142:337–51.

- [32] Michels H, Pitz-Paal R. Cascaded latent heat storage for parabolic trough solar power plants. *Sol Energy* 2007;81(6):829–37.
- [33] Elfeky K, Ahmed N, Wang Q. Numerical comparison between single PCM and multi-stage PCM based high temperature thermal energy storage for CSP tower plants. *Appl Therm Eng* 2018;139:609–22.
- [34] Flueckiger SM, Garimella SV. Latent heat augmentation of thermocline energy storage for concentrating solar power – a system-level assessment. *Appl Energy* 2014;116:278–87.
- [35] Wakao N, Kagei S. Heat and mass transfer in packed beds. Taylor & Francis; 1982.
- [36] Zanganeh G, Khanna R, Walser C, Pedretti A, Haselbacher A, Steinfeld A. Experimental and numerical investigation of combined sensible-latent heat for thermal energy storage at 575 °C and above. *Sol Energy* 2015;114:77–90.
- [37] Kind M, Martin H, Stephan P, Roetzel W, Spang B, Müller-Steinhagen H, et al. VDI heat atlas. 2010.
- [38] Wakao N, Kaguei S, Funazkri T. Effect of fluid dispersion coefficients on particle-to-fluid heat transfer coefficients in packed beds: correlation of Nusselt numbers. *Chem Eng Sci* 1979;34(3):325–36.
- [39] Incropera FP, Dewitt DP, Bergman T, Lavine A. Introduction to heat transfer. New York: John Wiley & Sons. Inc; 1996.
- [40] Beek J. Design of packed catalytic reactors. *Advances in Chemical Engineering*. Elsevier; 1962. p. 203–71.
- [41] Gonzo EE. Estimating correlations for the effective thermal conductivity of granular materials. *Chem Eng J* 2002;90(3):299–302.
- [42] Incropera FP, DeWitt DP, Bergman TL, Lavine AS. *Fundamentals of heat and mass transfer*. New York: Wiley; 1996.
- [43] Gunaratne DS, Chmielewski JK, Yang W. Pressure drop prediction of a gasifier bed with cylindrical biomass pellets. *Appl Energy* 2014;113:258–66.
- [44] Jegadheeswaran S, Pohekar S, Kousksou T. Exergy based performance evaluation of latent heat thermal storage system: a review. *Renew Sustain Energy Rev* 2010;14 (9):2580–95.
- [45] Elfeky KE, Mohammed AG, Wang Q. Numerical investigation of cycle cut-off criterion on system performance of thermocline tank. *Chemical Engineering Transactions* 2020;81:499–504.
- [46] Elfeky KE, Mohammed AG, Wang Q. Numerical study on the performance of thermocline tank for hybrid solar tower power plants using DEM-CFD coupled method. *Chemical Engineering Transactions* 2020;81:505–10.
- [47] Wang W, He X, Shuai Y, Qiu J, Hou Y, Pan Q. Experimental study on thermal performance of a novel medium-high temperature packed-bed latent heat storage system containing binary nitrate. *Appl Energy* 2022;309:118433.